Proceedings of the 11th ICPMG 2026
11th International Conference on Physical Modelling in Geotechnics
8-12 June 2026, Zurich, Switzerland

Modelling high-velocity pile uplift in saturated sand in laboratory tests

M. Cramer, F. Williams-Riquer
Institute of Geotechnical Engineering and Construction Management, Hamburg University of Technology, Hamburg, Germany, mechthild.cramer@tuhh.de

M. A. Pick
Institute of Mechanics and Ocean Engineering, Hamburg University of Technology, Hamburg, Germany

J. Grabe
Institute of Geotechnical Engineering and Construction Management, Hamburg University of Technology, Hamburg, Germany

ABSTRACT: Dynamic tensile loading frequently affects piles in offshore environments, where rapid loading conditions, such as vibrodriving, facilitate suction at the pile tip. While soil deformation beneath the pile tip during vibratory driving has been investigated using particle image velocimetry (PIV), this method cannot directly resolve cavity formation during rapid uplift, which therefore remains insufficiently understood. This study presents a laboratory test setup that enables the investigation of high-velocity pile uplift in fully saturated sand. Three representative upward motions are selected based on field tests and approximated to define a simplified laboratory input signal. The field tests use a model vibrodriver and are evaluated to characterise pile uplift motion during vibratory driving. The laboratory test stand enables extraction tests on model piles at velocities up to 3 m/s to reproduce the three representative upward strokes. The experimental setup includes sensors to measure the extraction force and the total and pore pressures directly beneath the pile tip. Results demonstrate laboratory reproduction of the upward motions observed in the field and show that rapid extraction reduces the pressure beneath the pile tip below hydrostatic equilibrium, while tensile force increases with extraction acceleration and velocity. The proposed approach provides a controlled basis for further laboratory-scale studies to better understand processes at the pile tip during vibratory driving and their implications for pile resistance.

1 INTRODUCTION

Vibratory pile driving enables fast installation with reduced noise emissions and a lower risk of structural damage to the pile than impact driving. Installation parameters govern the lateral and axial bearing capacity, during vibratory driving, with studies identifying frequency (Achmus et al., 2020; Hartung, 1994), soil density (Peccin Da Silva et al., 2023; Vipulanandan et al., 1990), and crane load (Peccin Da Silva et al., 2023; Stein, 2023) as relevant factors. Beyond their impact on capacity, these parameters also influence the installation process. The force ratio of the dynamic vibratory force and the static load (including crane load) also influences the penetration rate during vibratory pile installation (Martinelli et al., 2025; Hein Mazutti et al., 2026). The mechanism of vibratory pile driving is commonly described as a temporary reduction in shaft and toe resistances caused by cyclic shearing and the generation of excess pore pressure in the surrounding soil (Heerema, 1978; Jonker, 1987). In granular soils, vibratory driving induces particle rearrangement and temporary loss of effective strength. Jonker (1987) introduced the term *soil resistance during vibratory driving* (SRV), which represents the vibratory driving resistance by relating it to the static pile resistance through constant reduction factors β. Several authors also describe a fluidised or pseudo-fluidised zone around the pile during vibration (Holeyman, 2002; Rodger and Littlejohn, 1980; Viking, 2006), yet the detailed soil state within this zone remains unclear.

Rodger and Littlejohn (1980) distinguished between *slow* and *fast* vibratory driving based on whether the pile movement reverses during a cycle. Dierssen (1994) refined this classification by subdividing the slow mode into *slow* and *fast* driving. In his framework, slow vibratory driving is characterised by complete soil relaxation beneath the pile tip during upward movement. Dierssen (1994) labelled the mode with no reversal of motion (Rodger and Littlejohn's (1980) fast vibrodriving) *pulsing* driving. Cudmani (2001) introduced the terms *cavitational* and *non-cavitational* vibratory driving. In the cavitational mode, the pile tip separates from the soil during upward motion, allowing complete unloading of the soil beneath the tip. Non-cavitational driving includes all modes without such separation. The driving mode can be identified from the pile-head force-displacement response at the beginning of the downward movement. If the pile-head force does not increase over an initial displacement interval, this indicates motion within a cavity (gap) beneath the tip and negligible soil reaction. Only after this interval does the pile come into contact with the soil again, as indicated by an increase in pile-head force. In this work, we will use the terms cavitational and non-cavitational driving as they were defined by Cudmani (2001).

The nature of the gap beneath the pile tip that forms during cavitational driving is still unknown. Massarsch et al. (2022) reported that cavitational driving is commonly encountered in practice and emphasised that pile tip resistance governs penetration, as shaft resistance is strongly reduced by cyclic loading. If pile tip resistance governs penetration under these conditions, the soil-water response beneath the tip during rapid uplift is a key mechanism that remains poorly understood.

A possible mechanism discussed in the context of rapid upward pile movement in saturated sand is the generation of negative pressure beneath the pile tip. If the pile tip loses contact with the soil, a cavity may form and be filled by inflowing water due to pressure equalisation. The inflow may fluidise the soil and, under sufficiently low pressures, cavitation may occur. Physical cavitation could damage the pile material, thereby reducing the pile's bearing capacity. Experimental evidence for physical cavitation remains scarce, however numerical formulations can explicitly model the corresponding pile-soil separation states (Staubach and Machaček, 2023). Using digital image correlation, Vogelsang et al. (2016) identified the cavitational driving mode from the measured force signal. However, no pure water-filled cavity was observed at the pile tip; instead, the results indicate a soil-water mixture behaving like a viscous fluid. Maximum vertical soil displacement in the vicinity of the pile of around 40 % of pile displacement was recorded during cavitational driving (Vogelsang et al., 2017).

The conditions under which negative pressures beneath the pile tip lead to water inflow, soil fluidisation, or physical cavitation are still unclear. To enable controlled investigation of these processes, this paper presents an experimental approach to reproduce the upward stroke observed during vibratory driving under laboratory conditions.

The remainder of this publication is organised as follows. In Section 2, field tests with a model vibrodriver are analysed to characterise representative upward motions. To define a simplified laboratory input signal, three representative upward motions are selected and approximated. In Section 3, a test stand is introduced that can recreate upward motion from rest at field-representative velocities and accelerations. The planned soil conditions, including soil properties and sample preparation, are described in Section 4. In Section 5, the first results are presented, including the comparison between laboratory and field motions as well as the measured total pressures and axial forces.

2 FIELD TESTS

Field tests were conducted at a test site in the south of Hamburg. A tubular steel pile with a diameter of 3 cm was vibrated into the ground to depths of up to 70 cm using a model unbalanced vibrator. The test site soil consists of medium-dense fine sand with up to 10% fine contents (particle size < 0.063 mm) and is partially saturated. This vibrodriver allows manual adjustment of both the vibration frequency and the eccentric moment. During installation, the axial force above the pile, the total stress beneath the pile tip, the vertical displacement, and the installation parameters (frequency and eccentric moment) were measured. In total, four piles were installed to depths of approximately 70 cm. The frequency was varied between 20 and 30 Hz, while the eccentric moment was varied between 0 and 100%.

2.1 Vibratory driving mode

To classify the driving mode as cavitational or non-cavitational driving, the measured installation signals are evaluated. The analysis uses the vibrator displacement, the total stress beneath the pile tip, and the axial force measured by the load cell installed between the vibrator and the pile head (here termed pile-head force). The load cell acts as a stiff elastic element and records relative changes in dynamic tension-compression force.

In Figure 1, the comparison of non-cavitational driving (left; 1 & 3) and cavitational driving (right; 2 & 4) using normalised pile-head force-penetration curves (1 & 2) and normalised total-stress time histories (3 & 4) is shown. The force curves are normalised by the common maximum force, and the stress curves by the common maximal total stress; note that the plots differ in scale. Both modes occur as described by Cudmani (2001). In the cavitational mode, the pile-head force does not increase at the start of the downward movement (highlighted in subfigure 2), indicating pile motion within a gap. In this case, the total stress at the pile base drops to zero and remains there briefly constant (highlighted in subfigure 4), consistent with loss of contact. In the non-cavitational mode, contact is maintained, and no zero-stress plateau occurs (subfigure 3). Thus, both modes can be distinguished from the pile-head force, supported by the total-stress response.

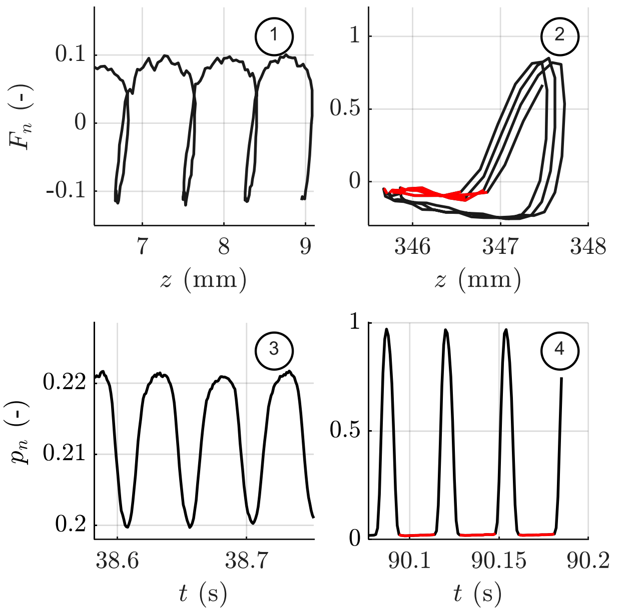

Figure 1. Force vs. displacement (1&2) and pressure at the tip vs. time (3&4) in non-cavitational (1&3) and cavitational (2&4) pile driving

2.2 Upward displacement at vibratory driving

During installation, displacement-time data of the vibrodriver were measured for a range of vibration frequencies and eccentric moments. The measurements were divided into sections with constant frequency and maximum eccentric moment. For each section, the mean upward displacement stroke $\bar{A}$ was derived from the signal (Figure 2). In Figure 2, the dashed vertical lines indicate the displacement range $2A_i$ between local minima and maxima. Following standard convention, the amplitude A_i is defined as half of this range. The mean stroke obtained for the entire dataset are shown in Figure 3. Small strokes occur at both low and high frequencies. Larger strokes are observed only at higher frequencies. However, no clear overall trend with frequency can be identified. The lack of a clear frequency-stroke relationship implies that other factors, such as penetration depth, soil conditions, or driving mode, also govern the uplift cycle.

These results provide ranges of upward displacements at different frequencies for laboratory reproduction of the upward stroke with field-representative kinematics. Three upward movements, representative of 20, 24, and 30 Hz, were selected for reproduction in the laboratory. The measured displacement signals are shown in black in Figure 4.

To reproduce these motions in the laboratory, the measured displacement signal must be simplified. In the following, the sinusoidal motion is approximated by a piecewise-defined profile with constant acceleration and constant velocity segments. This approximation is required by the acceleration- and velocity-controlled test stand described in Section 3.

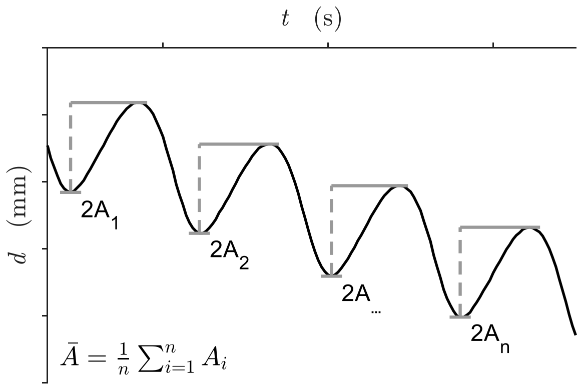

Figure 2. Schematic illustration of the calculation of the mean upward displacement amplitude

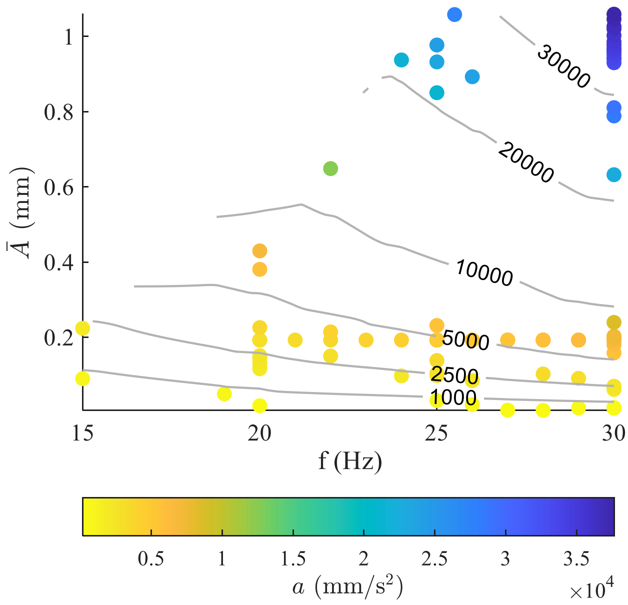

Figure 3. Resulting upward displacement amplitudes and accelerations from different frequencies during field tests

2.3 Three-phase approximation of sinusoidal upward motion

The laboratory test stand is controlled by prescribed acceleration and velocity. Therefore, the upward motion measured in the field is translated into a simplified input signal with piecewise acceleration and velocity. The upward part of the motion is considered from a local minimum at −A to the subsequent local maximum at +A. The upward stroke is approximated in three phases:

1. constant upward acceleration $+a$ over a duration T_1,
2. constant upward velocity v over a duration T_2,
3. constant downward acceleration $-a$ over a duration T_1,

with zero velocity at the start and at the end of the half-stroke (at $-A$ and $+A$). Two constraints are imposed to ensure comparability to the sinusoidal motion: (i) the total time of the three-phase profile equals half the vibration period π/ω, where $\omega = 2\pi f$ and f is the vibration frequency; and (ii) the total displacement over the half-period equals the change in amplitude, i.e. $2A$.

Under these constraints, the duration of the acceleration and deceleration phases is

$$T_1 = \frac{\pi-\sqrt{\pi^2-8}}{2\omega} \quad (1)$$

and the duration of the constant-velocity phase is

$$T_2 = \frac{\sqrt{\pi^2-8}}{\omega} \quad (2)$$

Assuming constant acceleration in the first phase, the acceleration is taken as

$$a = A\,\omega^2 \quad (3)$$

and the constant velocity during the second phase follows from

$$v = aT_1 = A\,\omega^2 T_1 = A\,\omega\frac{\pi-\sqrt{\pi^2-8}}{2} \quad (4)$$

Thus, once the frequency f and the corresponding upward stroke $2A$ are obtained from the vibratory tests, the idealised three-phase motion is entirely defined by T_1, T_2, a, and v. Figure 3 shows the accelerations computed from Eq. 3, indicating that for a given stroke the acceleration increases with frequency. In Figure 4, the approximation derived from Eqs. 1-4 with the measured displacement signals of the selected representative upward movements are compared. The corresponding input parameters (f, A, a and v) are listed in Table 1. In the laboratory, only the first two phases are applied: the constant-velocity phase is extended until the pile is fully extracted, and the deceleration phase is not reproduced. The field measurements show that the upward stroke varies with vibration frequency, but it is not solely determined by frequency. Additional factors, such as penetration depth, soil conditions, and driving mode, likely contribute to the observed scatter. Using the three-phase approximation, the measured strokes and frequencies were converted into corresponding acceleration and velocity ranges. These values define the target accelerations and velocities for the single-stroke extraction motions applied in the laboratory test stand.

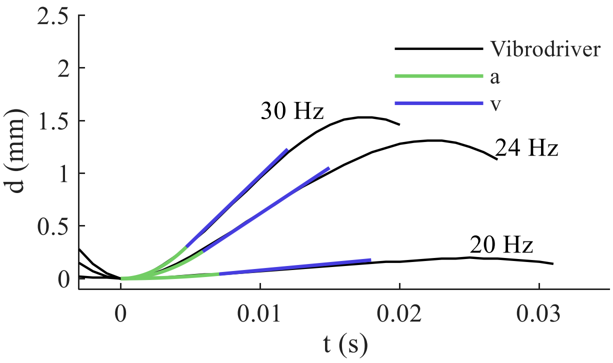

Figure 4. Approximation of the sinusoidal displacement signal assuming constant acceleration and velocity

Table 1. Properties of exemplary upward movements shown in Figure 4.

f (Hz)	A (mm)	a (mm/s²)	v (mm/s)
20	0.11	1737	12
24	0.655	14894	88
30	0.765	27181	128

3 TEST STAND SETUP

The test stand at the Hamburg University of Technology is an adapted version of a previous research setup (Nagula et al., 2022) and was modified to meet the requirements of this study.

3.1 Equipment and test sequence

The testing facility, shown in Figure 5, has a total height of 3.7 m and is supported by a rigid frame. The 3 cm diameter pile is connected to the linear motor rod (LinMot PS10-70), which enables maximum velocities of up to 3 m/s and maximum accelerations of up to 500 m/s², with a stroke of 40 cm. Because the limited force of 2.7 kN is insufficient to press the pile statically into the soil at low speed, the linear motor is mounted on a linearly actuated bridge structure. The maximum force of the bridge is 100 kN at a maximum speed of 70 mm/s, with a stroke of 100 cm. A mechanical holding brake can hold the rod of the linear motor in place to prevent unintended movement and ensure precise positioning between tests. The actuators are controlled using LabVIEW and a National Instruments CompactRIO controller.

With the linear motor blocked, the pile is pressed into the soil by the bridge at a constant penetration rate of 2 cm/s. After installation, a waiting period allows the pore pressure to dissipate. The pile is then unloaded to a predefined pre-load by lifting the bridge by a few millimetres; the brake still holds the pile in position. From the moment the brake is released, the linear motor maintains the pre-load force, and in the last step, it executes the highly accelerated upward motion with the prescribed acceleration and velocity.

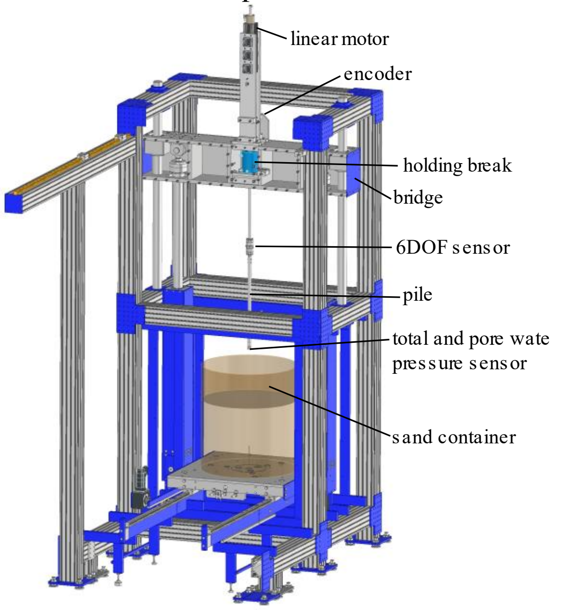

Figure 5. Test stand setup for fast extraction of piles in saturated sand

3.2 Measurement concept

The test stand is equipped with different sensors. Since the focus is on the water-soil-pile interaction at the pile tip, two piezoelectric pressure sensors (Kistler, Type 601C, pressure range 0 – 250 bar) are installed directly at the pile tip (see Figure 6). One is mounted flush with the tip surface to measure total pressure, while the other is positioned behind a sinter metal filter plate to capture pore pressure. The filter plate (GKN, SIKA-B 30) has a mean flow pore size of 18 µm, determined in accordance with ASTM E1294 (1989) using liquid-displacement porosimetry. This value represents the characteristic pore diameter derived from the pressure-flow response measured during the test. Above the pile's head, a six-degree-of-freedom (6-DOF) force-torque sensor (Kistler, Type 9306A, vertical force range -5 – 10 kN) is installed. The measured vertical force component serves as the primary driving force, whereas the remaining force and torque components are used to monitor deviations from vertical alignment. Pile displacement is measured over time using an encoder (Heidenhain LIC 4005) with a resolution of 1 nm, mounted on the linear motor rod. All sensors are fully synchronised to ensure consistent temporal resolution. Data were recorded with a sampling frequency of up to 50 kHz.

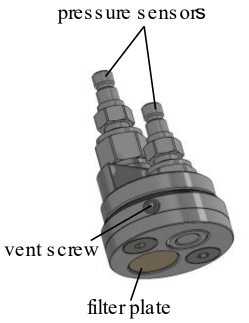

Figure 6. Pile tip with sensors and mounted filter plate

4 SOIL AND SAMPLE PREPARATION

Two sands, both predominantly composed of quartz, were selected as model materials: ISS0 sand is a fine sand, while Hamburg sand 2 (HS 2) is a medium sand. Both sands are commonly used at the research institute, where extensive experience and standardised test data are available for these materials. The main soil properties are summarised in Table 2.

Table 2. ISS0 and Hamburger Sand 2 material properties

Parameter	Symbol	ISS0	HS 2	Unit
Median grain size	D_{50}	0.164	0.646	mm
Coefficient of uniformity	C_u	1.73	1.45	-
Max. void ratio	e_{max}	1.038	0.883	-
Min. void ratio	e_{min}	0.599	0.618	-
Specific gravity	ρ_s	2.64	2.64	-
Friction angle	φ	29.8-33.3	37.6-44.2	°

The sand container used for testing is 100 cm high and 65 cm in diameter (Figure 5). It is filled with sand with a target relative density of $D_r = 85\%$ and covered with a 10 cm water layer. To obtain uniform and reproducible initial conditions, the soil is reconditioned before each test. Water is injected through a lance from the surface to the bottom, generating an upward flow that fluidises and loosens the sand. This approach fluidises the sand along defined vertical lines, ensuring a controlled and repeatable procedure. The methodology of injecting water from the bottom was discarded to avoid creating preferential flow paths and uncontrolled loosening. To compact the sand, a horizontally oscillating vibrator is applied at eight radially symmetrically arranged locations around the pile installation point (four at 10 cm and four at 20 cm distance from the centre), then slowly withdrawn to achieve uniform densification. The middle of the tank, where the pile is installed, is intentionally excluded from the compaction grid.

5 PRELIMINARY RESULTS

In this section, the first results on reproducing the field-measured upward movements with the laboratory test stand are presented. Three representative upward motions were replicated under controlled laboratory conditions in Hamburger Sand 2. The kinematic comparison is shown in Figure 7, and the corresponding total pressure beneath the pile tip and axial force at the pile head during the initial phase of the movement are shown in Figure 8.

The imposed kinematics are reproduced with high accuracy. Differences occur mainly during the deceleration phase, where the motions diverge.

At a displacement of 0 mm, the pile is at rest. The measured pressure at rest corresponds to atmospheric pressure plus the hydrostatic head of 0.40 m water. Pressures are reported in absolute scale. Values below the initial level indicate pressures lower than the hydrostatic equilibrium pressure.

The lowest pressure of 0.32 bar was measured for the fastest motion (approximated 30 Hz) beneath the pile tip. The corresponding tensile force of 480 N is more than three times higher than the maximum tensile force for the slower movement (20 Hz, 140 N). Minimum pressures and maximum tensile forces occur after the highest displacement within one vibration cycle.

The results show that rapid upward movements, as encountered during vibratory pile driving, cause a pressure drop beneath the pile tip to values well below the hydrostatic equilibrium pressure. Increasing acceleration and velocity increase the pressure drop. The lowest measured pressure remains above the physical cavitation pressure of water (23 mbar at 20°C). Physical cavitation was not observed in the experiments. However, larger displacement amplitudes reported in the literature for full-scale vibrators and piles (Rodger and Littlejohn, 1980; Stein, 2023) or less permeable sand may lead to pressure levels even closer to this limit under field conditions.

6 CONCLUSION AND OUTLOOK

This paper investigates the upward motion of a pile during vibratory driving in saturated sand. Field measurements were analysed to identify cavitational and non-cavitational driving and to quantify upward displacements. Subsequently, a laboratory test stand enabling rapid pile extraction and the project sands were presented. Finally, initial laboratory results showed that the test stand can reproduce the field-like

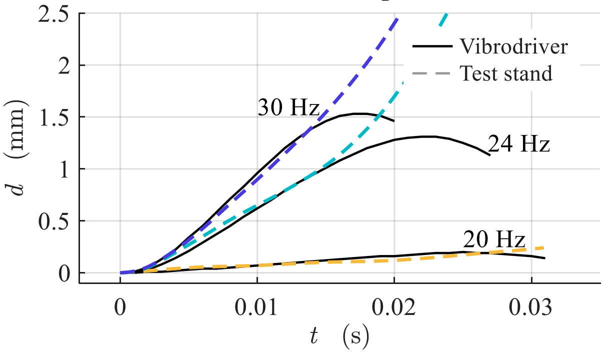

Figure 7. Comparison of the field-measured upward displacement and the laboratory reproduction using the test stand

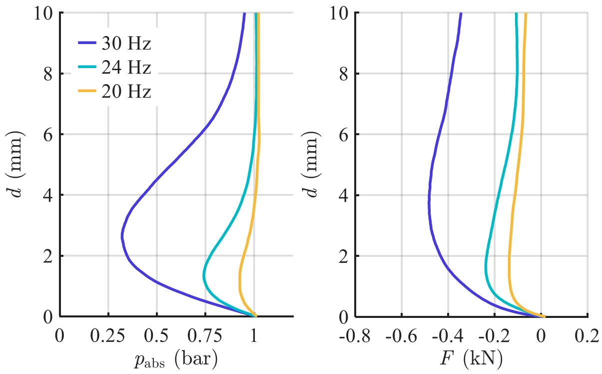

Figure 8. Pressure (left) and Force (right) at the beginning of the upward movement

upward motion for a single upward stroke and the correponding total pressure and force measruements. The main findings are:

1. The field tests confirm the occurrence of cavitational and non-cavitational driving as defined by Cudmani (2001). In particular, the measurements beneath the pile tip show that cavitational driving involves a temporary loss of contact, indicated by an interval of zero total stress at the pile tip.

2. The upward displacement amplitude is influenced not only by vibration frequency but also by additional factors that are not yet fully identified. The results suggest that soil conditions, penetration depth, and driving mode may play an important role.

3. The measured sinusoidal displacement can be represented well by an approximation with an initial phase of constant acceleration followed by a phase of constant velocity.

4. The test stand enables reproduction of upward motion observed in the field. Measurements show, that the fastest extraction led to a minimum total pressure

of 0.32 bar under the tip. Lower pressure than the hydrostatic equilibrium where measured in all experiments and can lead to a current in the piles tip direction which loosens up the soil.

5. Physical cavitation was not measured but cannot be excluded in real scale scenarios.

6. The required force to extract the pile gets higher with increasing acceleration and velocity. This trend may be linked to suction in saturated sand.

In future work, individual upward strokes will be reproduced systematically with the test stand and compared with laboratory-scale vibratory driving tests in saturated sand. The processes beneath the pile tip will be analysed for varying upward accelerations, velocities, and soil conditions, with particular attention to pressure and force development as well as pile–soil interaction.

ACKNOWLEDGEMENTS

The authors are grateful for the financial support provided by the German Research Foundation (DFG) – Project numbers 469320296 and 471875774

REFERENCES

Achmus, M., K. A. Schmoor, V. Herwig, and B. Matlock. (2020). Lateral bearing behaviour of vibro-and impact-driven large-diameter piles in dense sand. *geotechnik*, 43 (3): 147–159. https://doi.org/10.1002/gete.202000006.

ASTM E 1294 (1989). *Standard Test Method for Pore Site Characteristics of Membrane Filters Using Automated Liquid Porosimeters*. ASTM.

Cudmani, R. O. (2001). *Statische, alternierende und dynamische Penetration in nichtbindigen Böden.* PhD thesis, Universität Fridericiana in Karlsruhe.

Dierssen, G. (1994). *Ein bodenmechanisches Modell zur Beschreibung des Vibrationsrammens in körnigen Böden*. Phd thesis, Universität Fridericiana in Karlsruhe.

Hartung, M. (1994). *Einflüsse auf die Herstellung aud die Pfahltragfähigkeit in Sand*. Phd thesis, TU Braunschweig.

Heerema, E. P. (1978). Predicting pile driveability: Heather as an illustration of the 'Friction fatigue theory.' *European Offshore Petroleum Conference and Exhibition,* London. https://doi.org/10.2118/8084-MS

Hein Mazutti, J., Bienen, B., Bransby, M. F., & Randolph, M. F. (2026). Vibro-driven pile installation in sand performed in a geotechnical centrifuge. *Géotechnique*, 1-14. https://doi.org/10.1680/jgeot.24.01378

Holeyman, A. E. (2002). Soil behavior under vibratory driving. In: *Proceedings of the International Conference on Vibratory Pile Driving and Deep Soil Compaction*, Transvib 2002, 3–19.

Jonker, G. (1987). Vibratory Pile Driving Hammers for Pile Installations and Soil Improvement Projects. In: *Offshore Technology Conference*. Houston, Texas. https://doi.org/10.4043/5422-MS

Martinelli, M., Tsetas, A., Fărăgău, A. B., Metrikine, A., & Tsouvalas, A. (2025). Soil resistance during vibratory pile installation: Experimental findings from lab-scale tests. *Soil Dynamics and Earthquake Engineering*, *199*, 109692. https://doi.org/10.1016/j.soildyn.2025.109692

Massarsch, K., C. Wersäll, and B. H. Fellenius. (2022). "Vibratory driving of piles and sheet piles – state of practice." *Proceedings of the Institution of Civil Engineers - Geotechnical Engineering*, 175 (1): 31–48. https://doi.org/10.1680/jgeen.20.00127.

Nagula, S. S., J. Katt, and J. Grabe. (2022). "Optimisation of vibroflotation by amplitude in 1 g tests and coupled Eulerian–Lagrangian simulations." *International Journal of Physical Modelling in Geotechnics*, 22 (3): 143–156. https://doi.org/10.1680/jphmg.20.00083.

Peccin Da Silva, A., M. Post, A. S. K. Elkadi, E. Kementzetzidis, and F. Pisanò. 2023. Effect of Installation Parameters and Initial Soil Density on the Lateral Response of Vibratory-Driven Monopiles: A Laboratory Study. In: *9th International SUT Offshore Site Investigation Geotechnics Conference Proceedings "Innovative Geotechnologies for Energy Transition." Society for Underwater Technology. https://doi.org/10.3723/LFBS1210*

Rodger, A. A., and G. S. Littlejohn. (1980). A study of vibratory driving in granular soils. *Géotechnique*, 30 (3): 269–293. https://doi.org/10.1680/geot.1980.30.3.269.

Staubach, P., and J. Machaček. (2023). Separating fluid and solid contact constraints for hydro-mechanically coupled finite elements discretising fluid displacement." *Computer Methods in Applied Mechanics and Engineering*, 416: 116451. https://doi.org/10.1016/j.cma.2023.116451.

Stein, P. (2023). *Stress state developments during the installation of pipe piles in sand and their influence on the lateral load-bearing behaviour*. PhD thesis, TU Braunschweig.

Viking, K. (2006). The vibratory pile installation technique. *TRANSVIB 2006. Gonin, Holeyman et Rocher-Lacoste (ed.) 2006, Editions du LCPC*, Paris, 65–82.

Vipulanandan, C., D. Wong, and M. W. O'Neill. (1990). Behavior of Vibro-Driven Piles in Sand. *Journal of Geotechnical Engineering* 116 (8). https://doi.org/10.1061/(ASCE)0733-9410(1990)116:8(1211

Vogelsang, J., G. Huber, and T. Triantafyllidis. (2017). Experimental Investigation of Vibratory Pile Driving in Saturated Sand. *Holistic Simulation of Geotechnical Installation Processes, Lecture Notes in Applied and Computational Mechanics, edited by T. Triantafyllidis,* 101–123.

Vogelsang, J., G. Huber, T. Triantafyllidis, and T. Bender. (2016). Interpretation of Vibratory Pile Penetration Based on Digital Image Correlation. *Holistic Simulation of Geotechnical Installation Processes, Lecture Notes in Applied and Computational Mechanics, edited by T. Triantafyllidis*, 31–51.